Micro-Scale Modeling of Matrix-Fracture Interactions in Fractured Porous Media

Samuel Kazmouz[a], Maziar Arshadi[a], Arash Aghaei[b], Mohammad Piri[a],

a) Department of Chemical and Petroleum Engineering. University of Wyoming, Laramie, WY 82071-2000, USA.
b) Americas Oil and Gas, FEI Company, Houston, TX 77084

This paper was prepared for presentation at the International Symposium of the Society of Core Analysts held in Snowmass, Colorado, USA, 21-26 August 2016

ABSTRACT

In this study, we utilize a fully dynamic pore-scale network model to upscale two-phase flow from pore to core in fractured porous media. The key features of the model used include incorporation of viscous, capillary, and gravity pressure drops, accounting for wetting-phase corner flow in elements with angular cross sections, the ability to adjust the corner interfaces between wetting and non-wetting phases based on changes in local capillary pressures, and heavy parallelization. We utilize a miniature fractured Berea sandstone core with the fracture extending from the inlet to the middle of the core. The core is scanned using X-ray microtomography (micro-CT) imaging techniques at pore-scale resolutions. Two networks are generated from the processed micro-CT images; one for the matrix and another for the fracture. The two networks are then merged statistically based on actual matrix-fracture connections in the sample core, acquired after segmenting the matrix pores and fracture opening in the CT images. Oil-displacing-brine (drainage) and brine-displacing-oil (imbibition) processes are simulated through the fractured core. Primary results of the model, including fluid saturation and configuration at different locations within the fracture and the matrix, are then discussed. The model results are then used to draw a better understanding of multi-phase flow through matrix pores and fracture aperture.

INTRODUCTION

Multi-phase flow in porous media, in a petroleum engineering context, is the basis to predict fluid-rock properties (such as relative permeability curves) which are crucial for accurate predictions of reservoir performance. Pore network models, a form of pore scale modelling, transform the pore space into a representative pore-throat network which preserves its properties. Displacements are carried throughout the network in order to predict multi-phase flow [1]. Pore network models were introduced in the 1950s and have improved immensely since then [2]. The knowledge of pore scale physics has also

improved and while the majority of previous models were quasi-static, models now are fully dynamic and better represent the flow in the vicinity of the well bore [1].

While previous work has explored two-phase fully dynamic models in a porous rock [1] as well as isolated single fractures [3], we will take advantage of this study to explore fracture-matrix interactions. Fractures exist naturally in porous media and affect both its conductivity and continuity. Natural fractures were typically modeled using the dual-porosity approach and assigned straight line relative permeabilities. This approach is not sufficient and induces significant errors when predicting the performance of the fractured porous media [4]. Hence, in this work we use an accurate fracture aperture map as well as Berea Sandstone pore network, both constructed from real micro-CT images of a fractured core. The matrix and the fracture are then joined to create a single pore network which is representative of the fractured core. Two phase immiscible flow is then simulated using a fully dynamic model presented previously in [1]. The simulation results are then used to draw conclusions about the fracture, the matrix, and their interaction.

MODEL

In this paper, we use a fully parallelized model previously presented in [1] as a two-phase fully dynamic pore network model. It is a pore-to-core up scaling model which assumes Newtonian, incompressible, and immiscible fluids, where there is no diffusion between phases. In addition, network elements can be both, angular and non-angular. The model accounts for piston-like, snap-off, and pore-body filling displacements. It also includes wetting phase corner flow, simultaneous injection of the wetting and non-wetting phases, and a constant outlet pressure. The simulations start with fully saturated pores and throats. All possible displacements, based on accessibility are listed. Then, the displacements proceed from the highest to the lowest potential. After each displacement, the list is updated because new pores are now accessible. Displacement potential includes viscous, capillary, and gravitational effects and is described in Eq. 1 [1]. For a displacement to occur, displacement potential should be greater than zero. This means that the pressure of the invading phase needs to overcome the pressure of the defending phase and the pressure drop that would be incurred by the displacement.

$$\Phi_{disp}=P^{invd,\ inlet}-P^{def,\ outlet}-\Delta P^{disp}$$

In order to evaluate the displacement potential, the pressure field needs to be known. The pressure field is calculated by solving a system of linear equations (by using the MUMPS package), which is created by writing a volume balance for each pore-throat-pore configuration [1].

The model utilized accounts for a wetting phase in the corner, which in turn allows for snap-off displacement. Throughout the simulation, capillary pressure in the pore changes and this might move the location of the AM [1]. It is also important to add that the contact angles input into this model were measured in-situ, after experiments (refer to Fig. 1).

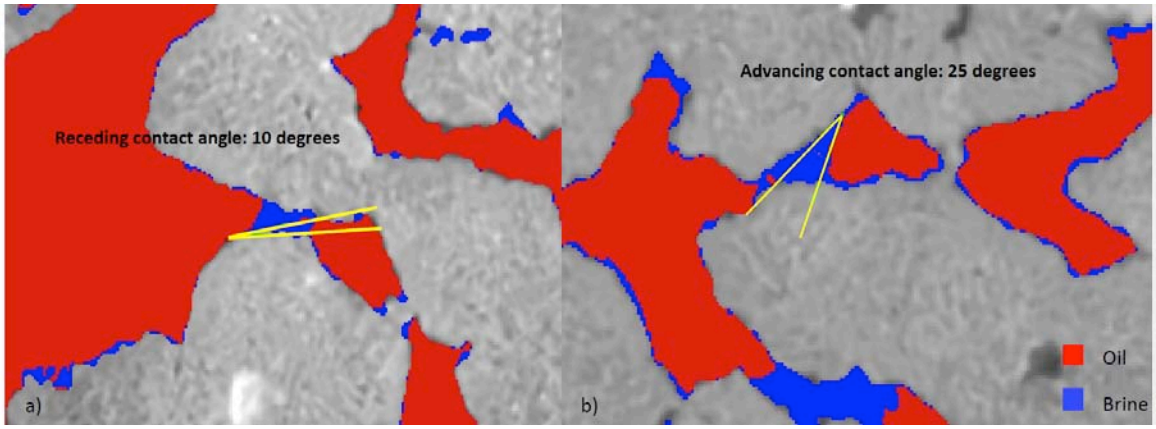

Figure1: In-situ measurements of brine-oil contact angle in pore space in the Berea sandstone core sample.

NETWORK REPRESENTATION OF THE FRACTURED POROUS MEDIA

In order to construct the network for this work, a fractured Berea sandstone core was scanned with a 2.5 μm resolution using high resolution X-ray CT scanner. The fractured core has a length of 53.9 mm and a diameter of 10 mm, while a fracture of width 10 mm, extends from the inlet to the middle of the core (Fig. 2-a). In order to study matrix-fracture interactions, in this work we select the region of the core where the fracture ends. As a result, a cylindrical subdomain (6 mm diameter, 6 mm long), which includes part of the fracture, was then extracted from the original scans (Fig. 2-b). These images were then segmented using histogram thresholding method. Histogram thresholding is a widely-used method for image analysis [5]. Maximum ball algorithm [6] was then used to generate the matrix pore network (Fig. 2-c), while the fracture pore network was generated using the aperture map of the real fracture, by converting the voxels of the CT images into a representative pore-throat network which preserves the properties of the fracture, such as connectivity. (Fig. 2-d). The two networks (matrix and fracture), were then connected statistically based on real number of connections between the fracture and matrix obtained from the fractured core scans to create the final network which includes both the matrix and the fracture as one pore network (Fig. 2-e). The final network has a diameter of 6 mm and a length of 6 mm, while the fracture has a width of 6 mm and extends 2 mm from the inlet into the core. The total number of elements in the final network is 511406 with 167707 being pores and 343699 being throats. In addition, Table. 1 lists the properties of the pore network.

Table 1: Properties of the pore network

Property	Fracture	Matrix	Total(with connections)
Pores	91405	49396	167707
Throats	178657	106587	343699
Total elements	270062	155983	511406
Pore space volume ($m^{3)}$	7.15×10^{-10}	2.66×10^{-8}	2.7315×10^{-8}
Percent pore space volume (%)	2.618 %	97.382 %	100 %

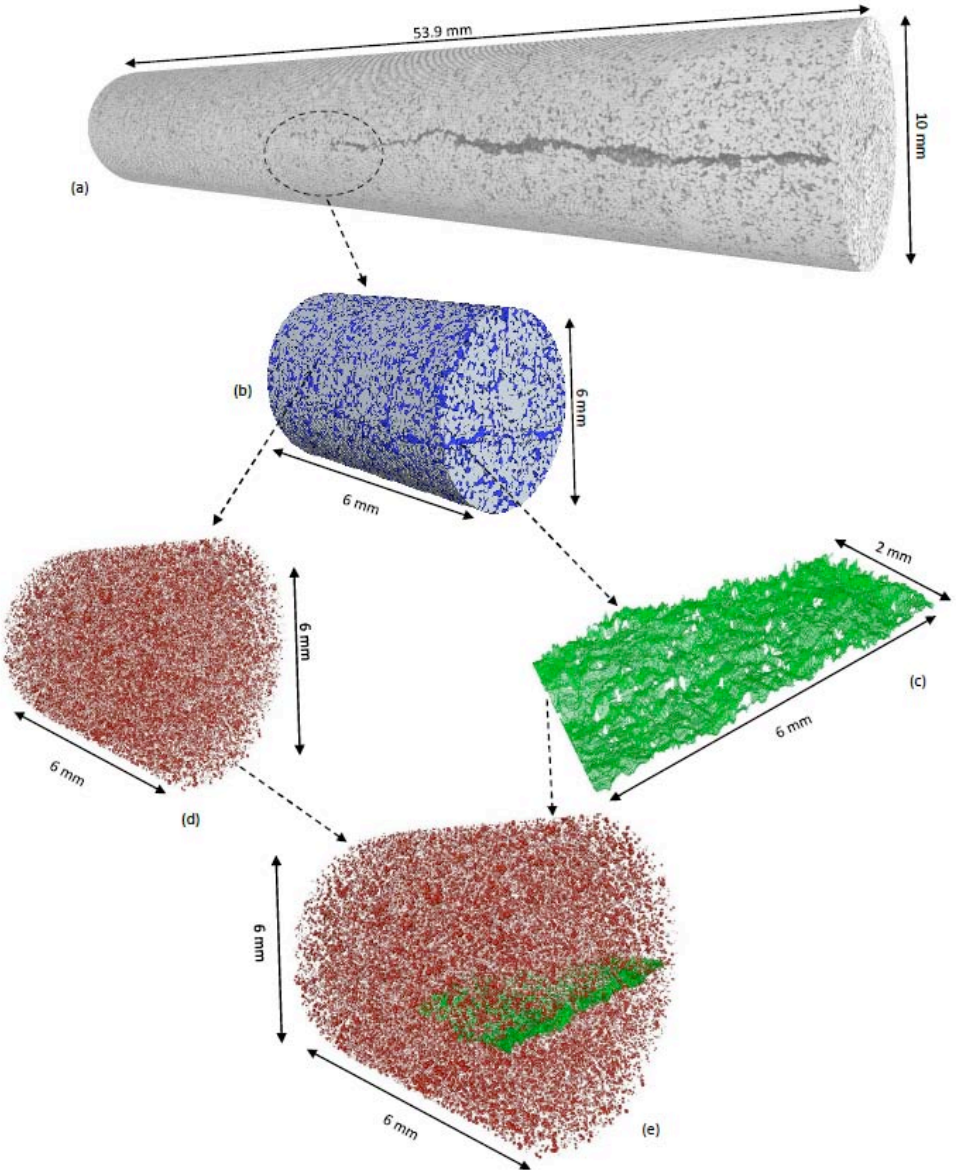

Figure2: Pore network construction stages

RESULTS AND DISCUSSION

Flow through the core sample described in section 3 was simulated using the model explained in section 2. Every simulation consisted of eighteen flow steps where brine and oil were injected simultaneously into the core. The medium was water wet and initially saturated with brine. At every step, the flow rates of brine and oil were increased or decreased depending on the type of flow process being simulated. Increasing oil flow rate while decreasing brine flow rate simulated drainage. On the other hand, increasing brine flow rate and decreasing oil flow rate simulated imbibition. In this work, two simulations were performed. Both simulations had the exact first nine steps, where drainage was maintained. However, for the final nine steps, the flow rate of brine was increased hundred times in the second simulation, compared to that of the first simulation. The first and second simulations are referred to as Sim.1 and Sim.2. The flow rates and the capillary numbers of each simulation can be seen in Table 2.

Table 2: Flow rates and capillary numbers of Sim.1 and Sim.2

Flow step	Oil flow rate (Sim.1, Sim.2) (m^3/s)	Brine flow rate (Sim.1) (m^3/s)	Brine flow rate (Sim.2) (m^3/s)	Oil capillary number (Sim.1, Sim.2)	Brine capillary number (Sim.1)	Brine capillary number (Sim.2)
1	1.667E-11	1.667E-09	1.667E-09	2.78E-06	3.65E-04	3.65E-04
2	8.333E-11	8.333E-10	8.333E-10	1.39E-05	1.82E-04	1.82E-04
3	1.667E-10	3.333E-10	3.333E-10	2.78E-05	7.29E-05	7.29E-05
4	3.333E-10	1.667E-10	1.667E-10	5.55E-05	3.65E-05	3.65E-05
5	6.667E-10	8.333E-11	8.333E-11	1.11E-4	1.82E-05	1.82E-05
6	1.333E-09	3.333E-11	3.333E-11	2.22E-04	7.29E-06	7.29E-06
7	1.667E-09	1.667E-11	1.667E-11	2.78E-04	3.65E-06	3.65E-06
8	3.333E-09	1.667E-11	1.667E-11	5.55E-04	3.65E-06	3.65E-06
9	6.667E-09	1.667E-11	1.667E-11	1.11E-03	3.65E-06	3.65E-06
10	3.333E-09	3.333E-13	3.333E-11	5.55E-4	7.29E-08	7.29E-06
11	1.667E-09	6.667E-13	6.667E-11	2.78E-04	1.46E-07	1.46E-05
12	8.333E-10	1.333E-12	1.333E-10	1.39E-04	2.92E-07	2.92E-05
13	3.333E-10	1.667E-12	1.667E-10	5.55E-5	3.65E-07	3.65E-05
14	1.667E-10	3.333E-12	3.333E-10	2.78E-05	7.29E-07	7.29E-05
15	8.333E-11	6.667E-12	6.667E-10	1.39E-05	1.46E-06	1.46E-04
16	3.333E-11	1.333E-11	1.333E-09	5.55E-06	2.92E-06	2.92E-04
17	1.667E-11	1.667E-11	1.667E-09	2.78E-06	3.65E-06	3.65E-04
18	0.000E0	3.333E-11	3.333E-09	0.000E0	7.29E-06	7.29E-04

FIRST SIMULATION - LOW FLOW RATE IMBIBITION

The first simulation is performed sequentially starting with the first step. Displacements are carried out until a steady state is achieved and no more changes are possible to the network fluid occupancy map. The capillary pressure (P_c), relative permeability (K_r), brine saturation (S_w), and occupancy per element of both oil and brine are written in output files, and then the solver proceeds to the second step. This algorithm is executed until all 18 flow steps are successfully simulated. The relative permeability curves of Sim.1 are presented in Fig. 3. Each point on Fig. 3 represents one flow step. S_w starts at around 82%, and drops to around 32% (initial brine saturation) at the end of drainage, then increases to 58% at the end of imbibition (residual oil saturation of 42%). The maximum K_{rw} exists at the first computed point of drainage (around 0.5), while the maximum K_{ro} occurs at the end of drainage (around 0.85). Fig. 3 shows that for a given saturation, K_{rw} and K_{ro} are, as expected, larger during drainage than during imbibition.

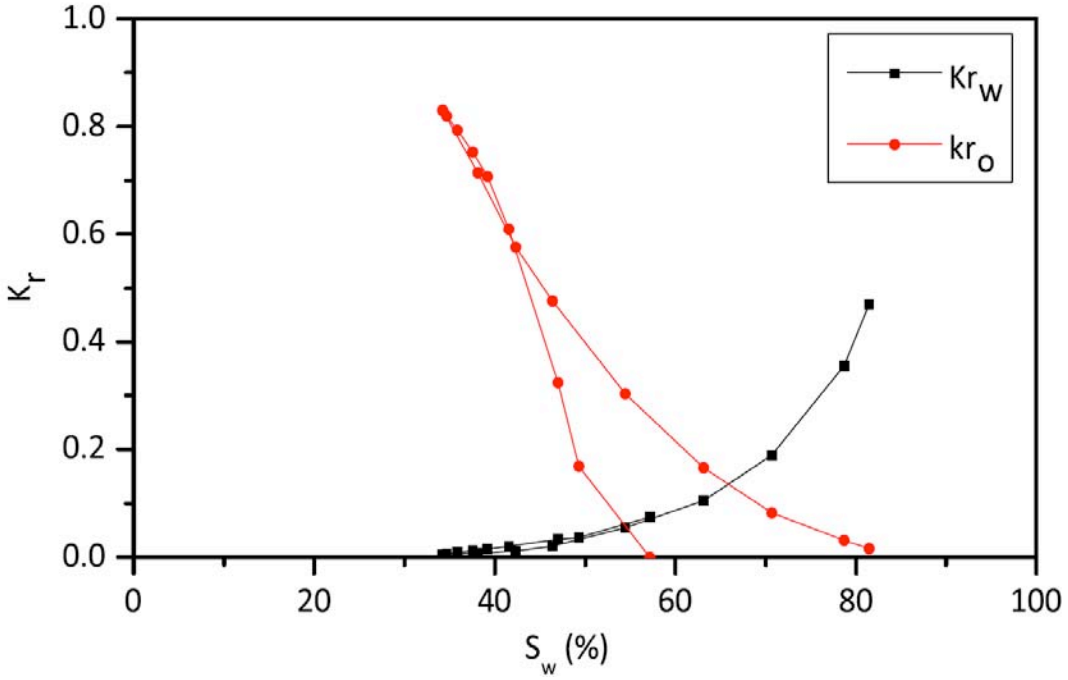

Figure 3: Relative permeability curves (Sim.1)

As stated earlier, the model writes out results files that hold the occupancy of each element (pore and throat) at the end of each flow step. The core sample is sectioned into 100 slices, and for each slice S_w and S_o are calculated for the matrix alone and the fracture alone portions (The saturation values were derived only using the center phase in the elements, and hence the results differ from those portrayed in Fig. 3. Since this is our first work in this field, the saturation profiles are used to compare trends, rather than actual values. Accurate saturation profiles which consider corner wetting phases, are in progress, and would be included in future work). Fig. 4 displays variations of S_w versus

the distance from the inlet for the matrix and the fracture, at the end of drainage and imbibition processes. As it is seen in this figure, the data of the fracture ends at a distance of 2 mm, which is the total length of the fracture network.

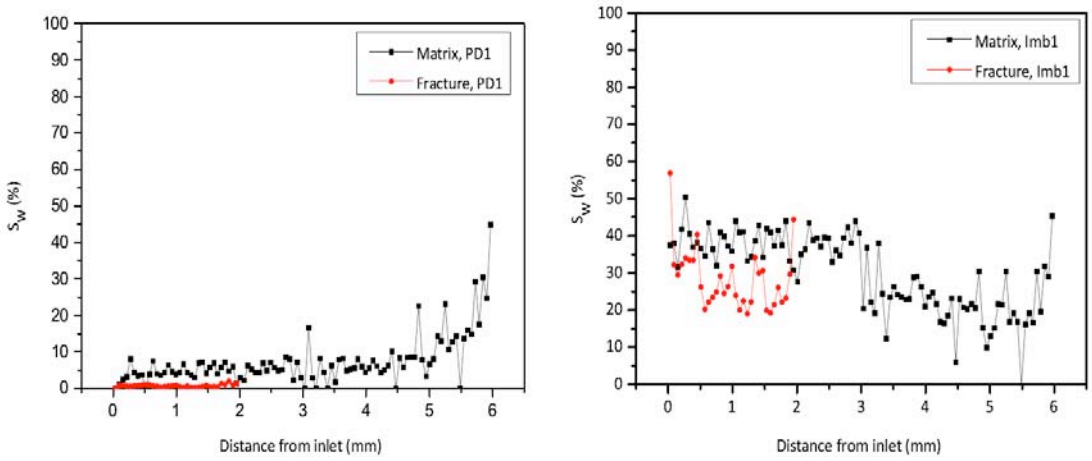

Figure 4: Water saturation (S_w) versus distance from the inlet for Sim.1

When considering drainage, it is expected that S_w will decrease in the network, since oil is displacing brine. Fig. 4-a shows that S_w drops to around 0% within the fracture, after drainage is complete, while S_w drops to around 5% in the region of the matrix closer to the inlet, but reaches values as high as 45% in the regions farther away from the inlet. This saturation profile is dependent on the aperture and pore size distributions in the fracture and matrix, respectively. During drainage, the largest elements are invaded first, due to their low threshold capillary pressure. The fracture includes large apertures (larger than the matrix pores), and hence it is favored for invasion by the oil. The final S_w in the fracture will be very close to 0% as the fracture is invaded completely by oil and brine only maintains wetting layers on the walls of the fracture, while brine remains in some pores and throats of the matrix depending on the oil flow rate, pore size distribution, and rock and fluid properties. In addition, as the oil flows through the network, it loses its viscous potential and hence the region of the matrix farthest away from the inlet will experience fewer displacements than those located closer, leading to a S_w being as large as 45% in regions close to the outlet.

Similarly, when considering imbibition, it is expected that S_w will increase in the network, since brine is displacing oil. Fig. 4-b shows that S_w increases to only 30% in the fracture due to of swelling of brine layers and snap-off mechanism that occurs in areas with small apertures. S_w in the matrix increases to around 40% in the sections closer to the inlet, and it drops to 20% in the regions farther away from the inlet. For imbibition, smaller pores are invaded first and hence the matrix is favored over the fracture when brine is displacing oil, and this leads to the matrix having higher S_w than the fracture. For the regions farther away from the inlet, the same reasoning for the lower S_w applies; the flow loses it viscous potential to invade the pores away from the injection site.

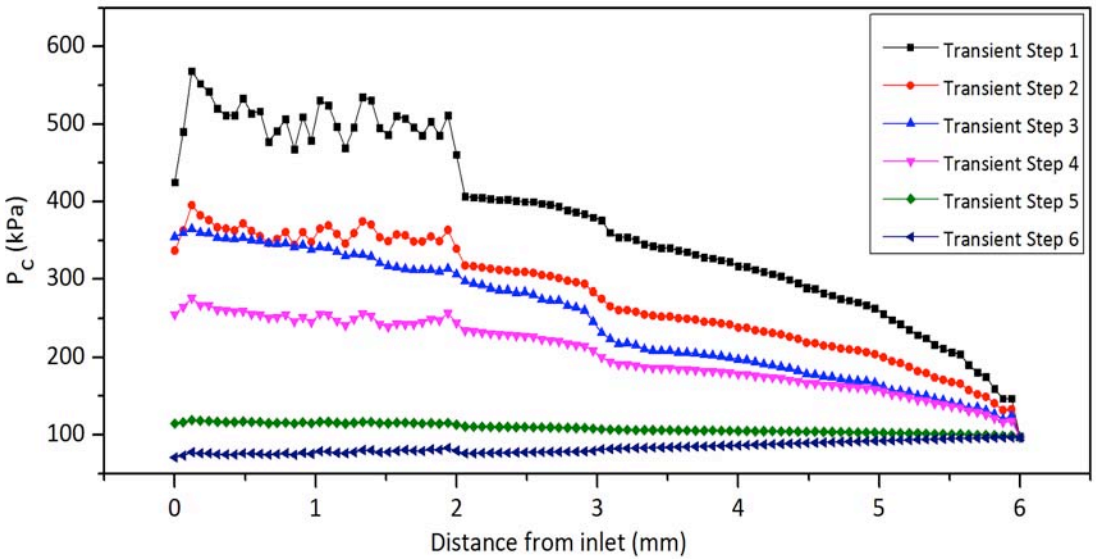

Figure 5: Capillary pressure (P_c) versus distance from the inlet (Sim.1)

As mentioned earlier, the difference between matrix pore sizes and the fracture apertures is the main factor affecting the differences in S_w. This becomes evident when the variation of capillary pressure with time is visualized. Fig. 5 shows the drainage capillary pressure P_c values versus the distance from the inlet, plotted for several time steps during the transient stage when displacements are still being carried out. The presence of the fracture within the matrix, and its subsequent effect on P_c is evident in the sharp drop of P_c in Fig. 5 "Transient Step 1", at a distance of 2 mm, which is exactly the length of the fracture. This happens because oil pressure is high at the inlet which causes a high capillary pressure. P_c experiences minimal drop within the fracture due to the large aperture, which does not reduce viscous pressure significantly. However, throughout the matrix, viscous pressure of oil drops, which leads to a drop in P_c As displacements are carried out, the system approaches steady state and P_c decreases, until it eventually becomes uniform throughout the core at around 50 Pa.

SECOND SIMULATION - HIGH FLOW RATE IMBIBITION

The second simulation proceeds in a similar manner as that of Sim.1, with the first nine flow steps being identical. Hence, at the end of drainage, the S_w profile was exactly the same as that seen in Fig. 4-a. However the flow rate for steps 10 through 18 for Sim.2 were 100 times larger than those of Sim.1. This meant that the results of this imbibition test were going to be different, and this can be seen in Fig. 6 that is a plot of S_w versus the distance from the inlet for the matrix and the fracture at the end of imbibition.

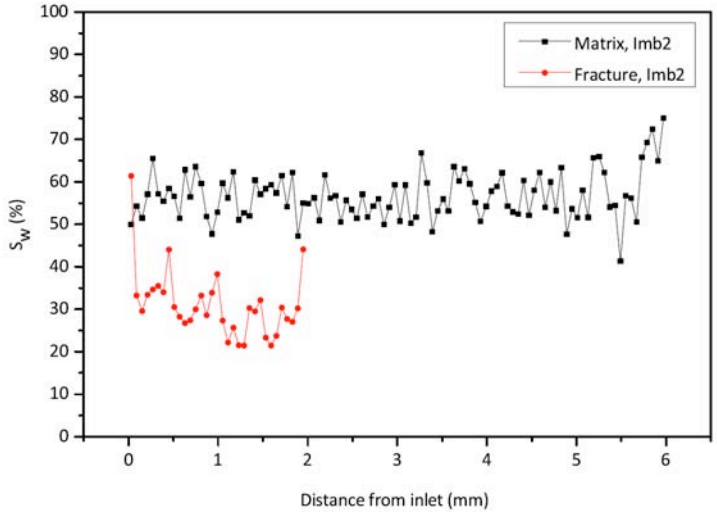

Figure 6: Water saturation (Sw) versus distance from the inlet, for imbibition (Sim.2)

Fig. 6 shows that S_w of the fracture is around 30% while that of the matrix is around 60% throughout the length of the core. The increase of flow rate in Sim.2 did not lead to a significant increase in S_w of the fracture, but caused S_w in the matrix to increase from 40% to 60% in the regions close to the inlet, and from 20% to 60% in the regions away from the injection site. This means that S_w in the matrix is not just greater, but more uniform across the length of the medium, when comparing the results of Sim.1 and Sim.2. The increased flow rate had enough viscous potential to uniformly displace the oil from the matrix. However, for the fracture, the increase in flow rate was not able to increase S_w, because the flow rate is still not large enough to overcome the threshold capillary pressure of the large aperture of the fracture. The increased flow rate might have caused the wetting brine layers in the fracture to swell, but not significantly enough to increase S_w appreciably.

CONCLUSION

In this study we utilized a fully dynamic pore network model to simulate drainage and imbibition processes in a fractured core, represented by a single pore network. The model utilized accounted for viscous, gravitational, and capillary effects. The pore network was constructed using micro-CT images of matrix and fracture in an actual fractured core sample. It was generated by connecting separate matrix and fracture pore networks. We performed two flow simulations each including drainage and imbibition steps. We used identical drainage steps in simulations to establish the same initial brine saturation distributions before inset of imbibition tests. The imbibition flow rates were significantly different. It was shown that at the end of drainage, the fracture was almost fully saturated with oil, while the matrix had some brine left in the corners and small pores (S_w of 5%). However after imbibition, the fracture S_w was resistant to changes in flow rate. For both simulations, S_w in the fracture was approximately 30%. On the other hand, water saturation in matrix showed significant sensitivity to changes in imbibition flow rate,

increasing from 20-40% to 60% from Sim.1 to Sim.2. Furthermore, water was distributed more uniformly throughout the length of the core at the end of imbibition in Sim.2. This was thought to be due to the increased flow providing sufficient pressure to establish efficient oil displacements in the entire core. It was shown that the presence of the fracture within the matrix increases P_c. A distinct change in P_c was observed along the medium where the fracture was present.

ACKNOWLEDGEMENTS

We gratefully acknowledge financial support of FEI, Saudi Aramco, Hess Corporation, and the School of Energy Resources at the University of Wyoming.

REFERENCES

[1] Aghaei, A. and Piri, M., "Direct pore-to-core up-scaling of displacement processes: Dynamic pore network modeling and experimentation", *Journal of Hydrology*, 2015.

[2] Karpyn, Z. T. and Piri, M., "Prediction of fluid occupancy in fractures using network modeling and x-ray microtomography. I: Data conditioning and model description", *Physical Review E*, 2007.

[3] Arshadi, M. and Khishvand, M. and Aghaei, A. and Al-Muntasheri, G. A. and Piri, M., "Micro-Scale Investigation of Matrix-Fracture Interactions in Fractured Porous Media", *Physical Review E,* 2016.

[4] Blunt M, "Flow in porous media--- pore-network models and multiphase flow", *Current Opinion in Colloid & Interface Science*, 2001.

[5] D. Wildenschild and AP. Sheppard, "X-ray imaging and analysis techniques for quantifying pore-scale structure and processes in subsurface porous medium systems.", *Advances in Water Resources*, 2014.

[6] Dong H, "Micro-CT Imagin and Pore Network Extraction", *Imperial College London*, 2007.